A Feature Selection Method for High Impedance Fault Detection

Qiushi Cui, *Member, IEEE,* Khalil El-Arroudi, *Member, IEEE,* and Yang Weng, *Member, IEEE*

Abstract—High impedance fault (HIF) has been a challenging task to detect in distribution networks. On one hand, although several types of HIF models are available for HIF study, they are still not exhibiting satisfactory fault waveforms. On the other hand, utilizing historical data has been a trend recently for using machine learning methods to improve HIF detection. Nonetheless, most proposed methodologies address the HIF issue starting with investigating a limited group of features and can hardly provide a practical and implementable solution. This paper, however, proposes a systematic design of feature extraction, based on an HIF detection and classification method. For example, features are extracted according to when, how long, and what magnitude the fault events create. Complementary power expert information is also integrated into the feature pools. Subsequently, we propose a ranking procedure in the feature pool for balancing the information gain and the complexity to avoid over-fitting. For implementing the framework, we create an HIF detection logic from a practical perspective. Numerical methods show the proposed HIF detector has very high dependability and security performance under multiple fault scenarios comparing with other traditional methods.

Index Terms—High impedance fault, distribution network, data mining, feature selection.

I. INTRODUCTION

HIGH impedance fault (HIF) normally exists in distribution power systems with voltages ranging from 4 kV to 34.5 kV. Upon the occurrence of HIF, its immediate vicinity is imposed with potential danger, which is hazardous to public safety. Unfortunately, HIFs cannot always be recorded in the fault report to relay engineers and the reported cases are therefore less than what line crews observe from the field. It was revealed in [1] that conventional protection cleared only 17.5% of staged HIFs. With renewable integration into the distribution grids, the importance of HIF detection increases dramatically. Therefore, an effective HIF detection method is required to avoid false tripping and maintain the continuity of power supply.

Specifically, an HIF is usually associated with an undowned or downed conductor. The undowned conductor scenario involves the contacts between overhead lines and tree limbs that have large impedance. Similarly, if a downed conductor falls on a poorly conductive surface such as sand, asphalt, grass, soil, and concrete, the fault current might be too low to reach the pickups of traditional ground overcurrent relays. Typical fault currents are reported ranging from 10 to 50 amps, with an erratic waveform [1].

It has been decades for researchers and engineers to seek for a universally effective solution to HIF detection. At the early stage, enhancements of conventional relays are proposed,

Qiushi Cui and Yang Weng are both with the School of Electrical, Computer and Energy Engineering, Arizona State University, Tempe, AZ, USA 85281. Khalil El-Arroudi is with the General Electricity Company of Libya, Tripoli, Libya. (E-mail: qiushi.cui@asu.edu; yang.weng@asu.edu; khalil.elarroudi@mail.mcgill.ca.)

leading to a proportional relaying algorithm [2], impedance-based method [3], and PC-based fault locating and diagnosis algorithm [4]. However, these methods are ineffective in detecting HIFs with a low fault current. For this problem, harmonics patterns are utilized to capture HIF characteristics, such as magnitudes and angles of 3rd and 5th harmonics [5], even order harmonic power [6], and interharnomic currents [7]. Besides, [8] proposes a Kalman-filter-based method to monitor harmonics in HIF detection. This type of methods actively injects higher than fundamental frequency signals like positive/zero voltage signals [9] into the grid to detect HIFs. Moreover, wavelet transform [10], genetic algorithm [11] and mathematical morphology [12] are proposed to detect HIFs. Unfortunately, most of these attempts at addressing HIF detection issues rely on simple thresholds and logic, which lacks a systematical procedure that determines the most effective features for various distribution systems and scenarios during HIFs. Therefore, it is getting necessary to introduce a systematic design for a learning framework so that information gain in high-dimensional correlation can be quantified for better HIF detections.

For learning, artificial intelligence such as expert system is proposed in the early 90's [13]. After this work, methods using neural networks [14], decision trees [15] and fuzzy inferences [11] are discussed in the subsequent years. In recent years, some data processing techniques including wavelet transform and mathematical morphology are gaining popularity in HIF detection. These techniques supply historical data to several machine learning algorithms (Bayes, nearest neighborhood rule, support vector machine (SVM), etc.) to differentiate fault cases [16]–[18].

Although the work above reveals the importance of machine learning in HIF detection, they only utilize a certain type of detection features on general HIFs. However, it is unlikely for a certain category to capture all characteristics of HIFs. Actually, various physical features from multiple types of signal processing techniques should be generated to explore the HIF pattern. In addition, the important step of feature selection should not be omitted before applying any learning algorithm. Otherwise, the historical data is not utilized enough for efficient learning in HIF.

This paper contributes to use variable-importance-based feature selection method to identify an effective feature set out from a large feature pool. Specifically, we conduct a systematic design of HIF feature pool by looking into when the fault happens, how long it lasts, and what the magnitude of the fault is. For when, we first calculate different quantities such as active power and reactive power based on the voltage and current time series. Then, we use the derivative of these quantities to tell when there is a potential change due to HIF. For how long, we use discrete Fourier transform (DFT)

to quantify the harmonics so those suspicious ones can be recorded for later inspection. For what magnitude, we employ Kalman Filter (KF) based harmonics coefficient estimation. Finally, power expert information is integrated into the pool, e.g., the angle difference between zero and negative sequence voltage. Finally, we focus on the power of feature extraction, information ranking, and detection logic, the merits of which keep unchanged under different HIF models.

In addition to the feature pool establishment, we also provide a framework for learning: feature ranking for maximizing information gain, HIF detection logic, and performance analysis. Inspired by the work in [19], we employ the elements in the confusion matrix and other associated evaluation criteria for performance comparison. These criteria enable the performance comparison with the existing high impedance fault detection techniques. Comparing to the signal processing techniques in [10]–[12], the applications of DFT and KF in this paper are mature, simple, cheap and reliable, which are widely deployed in present digital relays [20] and PMUs [21].

This paper is organized as follows: Section II introduces three types of HIF models. Section III, IV and V elaborate on the proposed systematical method of detecting HIFs, from the feature selection method to the generation of detection logic, and the suggested performance analysis. The conclusions are presented in the last section.

II. High Impedance Fault Modeling

Although HIF phenomena are difficult to model in general, there are mainly three ways to model HIFs including both downed and undowned types for analysis. Each way provides acceptable similarity with real HIFs from its own perspective. In the following, we briefly explain each of them and the motivation behind the chosen model.

- The first one is called the transient analysis of control systems (TACS) controlled switch, as proposed in [22]. This model emulates arc conduction, re-ignition, and extinction. The advantage of this model is the adjustable phase difference between the applied voltage and fault current.
- The second way originates from the Kizilcay model [23] which utilizes a dynamic arc model derived from the viewpoint of control theory based on the energy balance in the arc column [24].
- The third way of modeling HIF is the employment of two anti-parallel DC-sources connected via two diodes, plus two variable resistors. The nonlinear impedances was included to add the non-linearity of fault current [5]. Later on, the model is extended with two anti-parallel DC-sources connected via two diodes [25], which modeled the asymmetric nature, as well as the intermediate arc extinction around current zero. The above model was then modified by adding one [15] or two [17] variable resistances in series with the DC sources. This kind of model is able to model the effective impedance and thus the randomness of the resulting fault current.

In this paper, we employ the third model due to its easiness of implementation in Matlab Simulink for multiple simulations

to realize the proposed machine learning-based method. In addition, this model is further improved here by replacing the two variable resistors with two controlled resistors. Each controlled resistor has an integrator to represent the moisture changing process in the vicinity of the point of contact of the conductor with the ground, a randomizer to introduce more randomness during HIF and a first-order transfer function to tune the response to the introduced randomness.

Fig. 1 shows the HIF model used in this paper. This model connects one phase of the power line to the ground. Two variable resistors are both changing randomly and model the dynamic arcing resistance. Two sets of diodes and DC sources are connected in an anti-parallel configuration. The two DC sources are randomly varying as well, which model the asymmetric nature of HIF. The positive half cycle of HIF current is achieved when $V_{ph} > V_p$, while negative half cycle when $V_{ph} < V_n$. When $V_n < V_{ph} < V_p$, the current equals to zero, which represents the period of arc extinction. In order to generate a fault current down to 10 A in the benchmark system, we adopt the model settings in Table I.
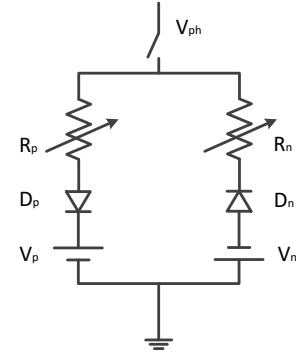

Fig. 1. HIF two anti-parallel dc-source model.

TABLE I
HIF MODEL PARAMETERS.

Component	Value range	Values change every
V_p	$5 \sim 6$ kV	0.1 ms
V_n	$7 \sim 8$ kV	0.1 ms
R_p	$30 \sim 1500$ Ω	0.1 ms
R_n	$30 \sim 1500$ Ω	0.1 ms

This model, therefore, becomes more accurate than the one in [17] since the moisture change and system dynamic response are incorporated. The obtained HIF current waveforms are presented in Fig. 2, which clearly displays the irregular, random, asymmetric and decreasing current waveforms upon the HIF. On the other hand, the course of arc extinction is depicted as well around small current in Fig. 3. It not only highlights the capability of the employed model on arc extinction modeling but also the asymmetric and nonlinear characteristics of the HIF. Through a harmonic decomposition of the measured HIF voltage signal, a total harmonic distortion of 0.31% is observed on the voltage signal and 24.99% is observed on the current signal in an ideal single phase circuit test. It makes sense that a HIF has a severely distorted fault current due to arcing and a not-much-compromised voltage

waveform regulated by the grid. Test results of this HIF model reveal a good modeling performance and are validated in the simulation [12] and field test results [26].
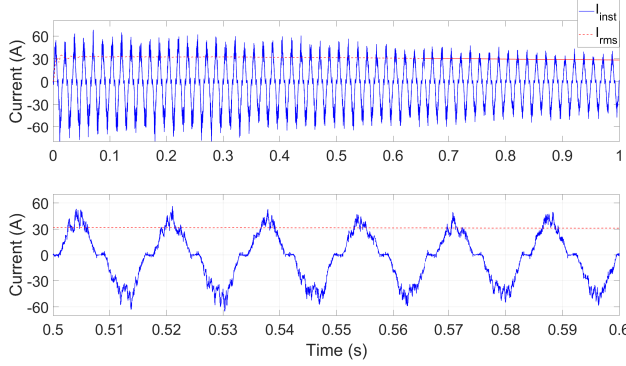

Fig. 2. The current waveforms upon HIF. The upper waveform shows the instantaneous and RMS HIF currents during 1 sec. The lower waveform is zoomed in from the upper waveform from 0.5 to 0.6 sec.
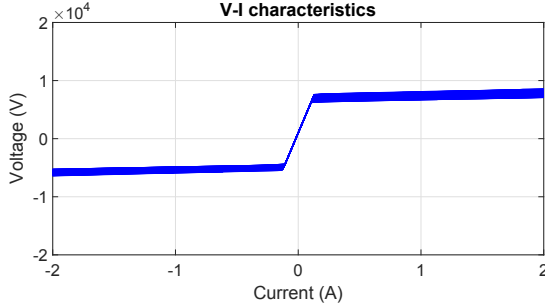

Fig. 3. HIF V-I characteristics.

III. FEATURE SELECTION METHOD FOR HIGH IMPEDANCE FAULT

Feature selection helps HIF detection identify key feature set and reduce data amount/layers, which increases the applicability of the method. Therefore, we elaborate on the way of selecting the key features in this section. The variable-importance in feature evaluation is firstly explained, followed by the pool of features and selected features. The way of obtaining the feature pool data is highlighted in the end.

A. Variable-importance in Feature Evaluation

The decision-tree-based algorithm in machine learning provides protection engineers with optimal relay logic and settings in distribution network protection [27]. However, it is of significant challenge to locate the key features of HIF given its randomness and irregularity. In other words, an effective and unbiased feature evaluator is required to calculate the merit of each tested feature before the classification between HIF event and non-HIF event. Here, we take advantages of the information gain and minimum description length (MDL)-based discretization algorithm to select important features during HIF. For the convenience of power background readers, we call MDL score the variable of importance in this paper.

The MDL-based method relies on the information gain (also known as entropy). Once the information gain of each feature

is calculated for the classification variable, those features that contribute more information will have a higher information gain value over others, whereas those that do not add much information will have a lower score and can be removed.

The score of variable-importance is one type of selection measures in machine learning. The problem of selecting the best attribute can be stated as the problem of selecting the most compressive attribute [28]. Assuming that all features are discrete, the objective is to find the best features that maximize the selection measure. "$n_{..}$" denotes the number of training instances and "$n_{i.}$" is the number of training instances from class C_i, $n_{.j}$ is the number of instances with the j-th value of the given attribute, and n_{ij} is the number of instances from class C_i and with the j-th value of the given attribute. Given C classes, the MDL can be defined as follows using the logarithm of all possible combinations of class labels:

$$\text{MDL} = \frac{1}{n_{..}}\Bigg(\binom{n_{..}}{n_{1.},\ldots,n_{C.}} - \sum_j \log\binom{n_{.j}}{n_{1j},\ldots,n_{Cj}}$$
$$+ \log\binom{n_{..}+C-1}{C-1} - \sum_j \log\binom{n_{.j}+C-1}{C-1}\Bigg) \quad (1)$$

In this paper, we use the MDL value to differentiate the merit of each detection feature for the classification between HIFs and non-HIFs. More details regarding how the variable-importance approach has been used in the feature evaluation for the HIF detection can be found in Appendix A.

B. The Pool of Candidate Features

In this study, 245 features are investigated as candidate features. For example, the feature pool in Table II is designed in four steps. Firstly, the time series data of voltage and current is obtained through with the DFT-based technique. Upon the aforementioned data, the feature pool is greatly expanded with multiple physical quantities through calculation in the second step. These calculated measurements range from the basic value (e.x. df, frequency) to the first order derivative (e.x. df/dt, the rate of change of frequency), considering both the absolute value and its changing rate. Thirdly, the harmonic coefficients are estimated through the KF-based technique, presenting the in-phase and in-quadrature components, i.e. $KF\_I\_sin\_H1$. Lastly, in order to capture some unconventional phenomena, some features are invented in the category of "other feature". For example, $\theta_{V_2} - \theta_{V_0}$, the angle difference between the negative and zero sequence voltage, is a good indicator of the unbalance level in distribution grids. Note that harmonic phase angles are in harmonic degrees and are the phase difference between the zero crossing of the fundamental frequency reference and the next zero crossing in the same direction of the harmonic.

Remark 1. *These features are extracted mainly through two techniques: discrete Fourier transform (DFT) and Kalman filter (KF). Both techniques are simple, reliable and implementable in engineering fields. The DFT is used to capture the majority of physical quantities in fault detection as is widely used in microprocessor-based relays. On the other hand, the utilization of the KF-based algorithm is motivated by the fact that it can accurately track the harmonics and inter-harmonics*

coefficients at given frequency components embedded in the input signals.

TABLE II
FEATURE POOL.

Feature Type	Designed Feature	Other Feature
DFT-based	$df, df/dt, P, dP/dt, pf,$ $dpf/dt, Q, dQ/dt, \phi, d\phi/dt,$ $H_{V1} \sim H_{V6}, H_{I1} \sim H_{I6},$ $V_{abc}, V_{012}, I_{abc}, I_{012}, dI/dt,$ $dV/dt, V_{ph}, V_{ll}, \theta_{V_{012}}, \theta_{I_{012}},$ $\theta_{H_{V1\_012}}, \theta_{H_{I1\_012}}$	$df/dP, df/dQ,$ $dV/dP, dV/dQ,$ $dH_{V1}/dt, dH_{I1}/dt,$ $\theta_{V_2} - \theta_{V_0}, \theta_{I_2} - \theta_{I_0}$
KF-based	$KF\_I\_cos\_H1 \sim H6,$ $KF\_I\_sin\_H1 \sim H6,$ $KF\_V\_cos\_H1 \sim H6,$ $KF\_V\_sin\_H1 \sim H6$	KF_V_DC

We are trying to include as many important and implementable features as possible. For instance, the parameters of "when" a HIF occurs such as the rate of change of active power (dP/dt) form a certain group of features in the feature pool. It actually does not matter if some non-HIF cases such as capacitor bank switching lead to similar changes since these cases only trigger certain features but not all features together in the proposed feature set or any well-trained statistical machine learning model. The reason for such choice is the adopted machine learning model might be so complicated that it needs the assistance of the "when" feature group at different thresholds for decision-making.

C. Systems and Events for Feature Selection

1) Benchmark System: The benchmark system utilized can be found in Fig. 4. The system configuration under different distributed energy resource (DER) technologies is presented in Table III. The wind farm is type 4 and rated at 575 V, 6.6 MVA. According to IEEE Standard 1547, the wind farm adopts constant power control with LVRT capability. The maximum fault current is limited to 1.5 pu.

TABLE III
SYSTEM CONFIGURATION UNDER DIFFERENT DER TECHNOLOGIES.

System Type	Location A	Location B
Synchronous-machine-based system	SG	N/A
Inverter-based system	WF	N/A
Hybrid system	SG	WF

SG, WF and N/A stand for the synchronous generator, wind farm and "not available" respectively.

2) Events Under Study: The technique is transferable on different feeders because the event category and event type in Table IV are suitable for most of distribution feeders during the training. Some of the event numbers are explained as follows. The 10 events from Type 1 is associated with the undowned conductor, where 3 SLG (AG, BG, CG), 3 LLG (ABG, ACG, BCG), 3 LL (AB, BC, AC), and 1 LLLG (ABCG) faults are included. The 3 events of Type 2 fault are the downed conductor for each phase. The fault impedance values includes $50, 150, 250, 350, 450,$ and $550\,\Omega$ in this paper. In load switching, the 6 types of non-fault events include 4 single

load switching (L-4, L-9, L-19, L-23) and 2 combinational load switching ((L-2,L-4,L-5) and (L-9, L-10)) events. The system loading for the normal state is shown in Appendix B. The 2 capacitor switching events have both the on and off status of the capacitor bank near bus B-15.

Moreover, the event category is flexible and can be tailored for other special systems by adding or deleting some of the event categories/types. In this case study, comprehensive scenarios are considered in the event category (refer to Table IV). A loading condition ranging from 30% to 100%, in a step of 10%, is simulated. Furthermore, eight loading conditions and three DG technologies are examined respectively on top of the base case scenario. Therefore, the number of fault and non-fault events are calculated as follows:

- Fault event: since two types of fault, summing up to 13 cases, are included, the number of fault events with one fault impedance, one fault location and one fault impedance is $(10+3) \times 8 \times 3 = 312$. Given 6 simulated fault impedances, 4 fault inception angles, and 3 fault locations, the total number of fault events add up to $312 \times 6 \times 4 \times 3 = 22464$.
- Non-fault event: it comprises normal state, load switching (adding and shedding) and capacitor switching events. Therefore the total number of non-fault events equals to $(1+6+2) \times 8 \times 3 = 216$.

The above event number results in an imbalanced dataset, where the number of data points belonging to the minority class ("non-fault") is far smaller than the number of the data points belonging to the majority class ("fault"). Under this circumstance, an algorithm gets insufficient information about the minority class to make an accurate prediction. Therefore, the synthetic minority over-sampling technique (SMOTE) is employed to generate synthetic samples and shift the classifier learning bias towards minority class [29].

TABLE IV
EVENT CATEGORY OF SYSTEM UNDER STUDY.

Event Category	Event Type	Number of Events
System Operating Condition	Loading Condition (30%-100%)	8
	DER Tech. (SG, inverter, hybrid)	3
Fault Event	Type 1: SLG, LLG, LL, LLLG	10
	Type 2: Downed conductor	3
	Fault impedance	6
	Inception Angle (0°, 30°, 60°, 90°)	4
	Fault location	3
Non-fault Event	Normal State	1
	Load Switching	6
	Capacitor Switching	2

3) Spatial data extraction: The HIF detection method should include spatial data by implementing current and voltage transformers and measurement devices at a substation and the downstream of the feeder. Knowledge extracted from these measurements is able to serve data from the spatial dimension for better detection coverage. Moreover, the proposed HIF detector installed along the distribution feeder is supplementary to the devices installed near the substation.
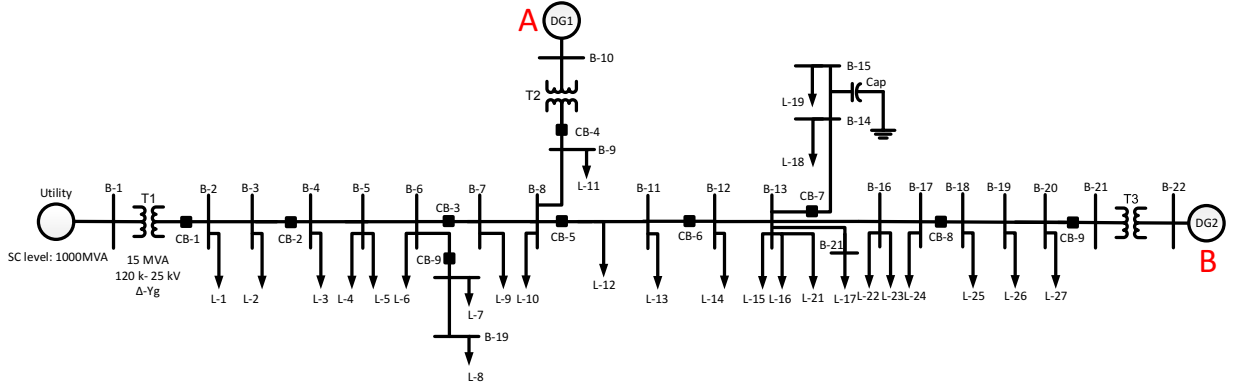
Fig. 4. Single line diagram of distribution feeder under study.

Since the further the HIF is to the substation, the lower the signal magnitude becomes if the HIF detector is installed near the substation. The signal sensitivity and accuracy issues are therefore addressed.

D. Effective Feature Set (EFS)

Finally, we propose an EFS in Table V after mining the collected data, applying the feature ranking algorithm and selecting the effective feature set (EFS) by considering the comprehensive performance in different distribution systems in Table III. The authors determine the cut-off point through a simple descending search process in the variable-importance list. A trade-off is realized between the detection performance improvement and the complexity of the detection logic. We start the search process by testing the first feature that has the highest score, then the first two features with the highest scores, then the first three and so on. Then we set two stopping criteria: (1) the incremental of detection accuracy (A, defined in Appendix C) of two adjacent tests is larger than 0.1%, and (2) the number of features is smaller than a practical number N ($N = 15$ is adopted in this paper). After extensive tests, we find that the increase of the performance indices becomes marginal when the variable-importance threshold is selected at 0.787. Meanwhile, the complexity of the detection logic and the number of signals are within an acceptable level (6 signals ignoring phases, three categories, suitable for unbalanced faults as shown in Table V).

According to the mathematical formulation and physical interpretation in Section III-A and III-B, the reasons that enhance these features to be used for the fault detection are (1) some physical quantities are statistically more relative to the classification results than others, and (2) based on the merit of each feature, the features in Table IV contribute more information gain than others. For example, $\theta_{V_2} - \theta_{V_0}$, the angle difference between the negative and zero sequence voltage, is selected since it captures the incremental of the unbalance level contributed from HIFs to distribution grids. The using of the angle difference between zero and negative sequence voltage is inspired by the work in [5], [30], and the practical engineering experience of the authors. To the best of our knowledge, this feature is utilized in some other fault detection application such as [30], but not in HIF detection before. Table VI shows the reference to the unbalanced fault detection features in EFS.

TABLE V
EFFECTIVE FEATURE SET OF HIF DETECTION IN THREE TYPES OF DISTRIBUTION SYSTEMS.

Fault Type	Proposed Feature
SLG, LL, LLG	$V_2, I_2, \theta_{V_2} - \theta_{V_0}, \theta_{I_2} - \theta_{I_0}$ $KF\_V\_cos\_H3, KF\_V\_sin\_H3$
LLLG	$V_{ll}, V_{ph}, H_{V1}, \theta_{H_{V1\_1}}$ $KF\_I\_cos\_H1, KF\_I\_sin\_H1$

TABLE VI
REFERENCE TO THE UNBALANCED FAULT DETECTION FEATURES IN EFS.

Feature in EFS	Reference
V_2	[5], [31]
I_2	
$\theta_{V_2} - \theta_{V_0}$	[30], [5]
$\theta_{I_2} - \theta_{I_0}$	
$KF\_V_a\_cos\_H3$	[5] (3rd harmonic), [8] (KF and low-order odd
$KF\_V_a\_sin\_H3$	harmonic), [32] (KF harmonic decomposition)

IV. HIGH IMPEDANCE FAULT DETECTION LOGIC

Inspired by the tree structure of the machine learning classifier model, the authors further explore the possibility of relating the EFS and the detection logic using simple thresholds as most of the commercial products [33] and patents do [34]. Statistically, since three-phase faults take up only $2\% - 3\%$ of the fault occurrences [35], an HIF detection logic is designed in this regard for unbalanced HIF only.

The HIF detection logic is targeted to be implemented in a microprocessor-based digital relay, as guaranteed by the selected feature selection techniques discussed in Section III-B. Similar to conventional digital relays, the proposed relay logic takes the voltage and current signals as its input. In addition, DFT and KF are required for corresponding feature extraction. Before the explanation of the HIF detection logic, the logic circuit is presented first in Fig. 5. Generally, the proposed HIF detection scheme updates its comparison and decision logic according to the obtained decision tree structure.

As indicated in the detection logic, three-phase voltage and current signals are sent to DFT and KF for feature extraction. This section takes the obtained EFS in Section III as an example. (2) and (3) show the extracted instantaneous signals after the DFT and KF blocks:
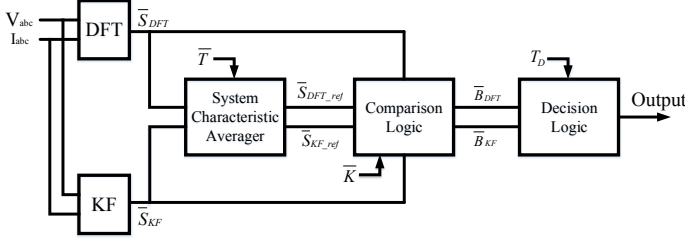
Fig. 5. The proposed HIF detection logic scheme.

$$\bar{S}_{DFT} = \{s_1, s_2\, s_3, s_4\} = \{V_2, I_2, \theta_{V_2} - \theta_{V_0}, \theta_{I_2} - \theta_{I_0}\} \quad (2)$$

$$\bar{S}_{KF} = \{s_5, s_6, s_7, s_8, s_9, s_{10}\} = \{KF\_V_a\_cos\_H3,$$
$$KF\_V_b\_cos\_H3, KF\_V_c\_cos\_H3, KF\_V_a\_sin\_H3,$$
$$KF\_V_b\_sin\_H3, KF\_V_c\_sin\_H3\}$$
$$(3)$$

A. System Characteristic Averager

The input of the System Characteristic Averager is the extracted instantaneous signals after the DFT and KF blocks. Meanwhile, the time duration $\bar{T}$ needs to be provided to this averager. Specifically, the System Characteristic Averager has a memory that stores the signals for a predefined duration of $\bar{T} = \{t_1, t_2, t_3, t_4, t_5, t_6,\, t_7, t_8, t_9, t_{10}\}$. In other words, $\bar{T}$ is the time constant that is a vector of ten elements associated with $\bar{S}_{DFT}$ and $\bar{S}_{KF}$. The input signals are stored and calculated at every $18,000$ cycles (5 minutes) [5]. After each batch of average value calculation, the system will automatically overwrite the earliest records once the storage capacity has been reached. The five minutes interval is subject to change depending on the case-specific analysis. Normally, the five-minute data is feasible for the distribution system condition evaluation and for modern digital relay implementation. For example, the HIF solution by SEL Inc. also deploys a memory function to record unusual signal changes related to system HIF [33], [36]. In-depth simulation or experimental results can be conducted to validate the effectiveness of this time constant over a large time scale. In the end, each time constant is either increased or decreased depending on the signal's slow or fast dynamic process.

To avoid signal spikes, a limiter is implemented at the beginning of each signal channel. Meanwhile, the time constant $\bar{T}$ is set according to the system characteristics of each individual signal. A small t_i ($i = 1, 2, \cdots, 10$) can avoid severe step change of signal but a large t_i costs more data storage and computational efforts. The output of the System Characteristic Averager block generates the reference value s_{i_ref} ($i = 1, 2, \cdots, 10$) for the Comparison Logic. A reliable average value is a prerequisite to successful detection.

B. Comparison Logic

The block of Comparison Logic is depicted in Fig. 6. Based on the feature extraction technique discussed in Section III, the extracted instantaneous signal s_i can be understood as the system background signal superimposed by the extra signal contributed from the HIF behavior. The comparison is therefore made between the extracted instantaneous signal s_i and its reference value s_{i_ref} [5].
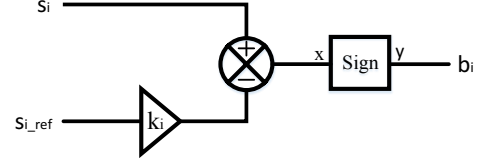

Fig. 6. Comparison Logic in the proposed HIF detection logic.

The sensitivity gain of k_i is incorporated in order to 1) set the margin of detection and 2) add a handle to the detection sensitivity. Where the undefined parameter of $\bar{K}$ stands for:

$$\bar{K} = \{k_1, k_2, k_3, k_4, k_5, k_6, k_7, k_8, k_9, k_{10}\} \quad (4)$$

The sensitivity gain $\bar{K}$ is set at 1.2 (adjustable for each element). The 20% above and below margin is adjustable and is taken as typical blackout region where the HIF tripping is not required [5]. This k_i value can be set to close to 1.0 after getting more confidence in HIF fault detection scheme. After the summation block in Fig. 6, a Sign function is employed to provide the following decision making:

- When $x > 0$, $y = 1$;
- When $x \leqslant 0$, $y = 0$.

The output of the comparison logic is the comparison assertion bit of b_i ($i = 1, 2, \cdots, 10$), the $\bar{B}$, which is the input to the decision logic.

C. Decision Logic

As mentioned in the previous subsection, the comparison assertion bit of b_i ($i = 1, 2, \cdots, 10$) is the output of the comparison logic in Fig. 6. The decision logic in Fig. 7, is the execution part of the HIF detection logic. There are four groups of signal bits:
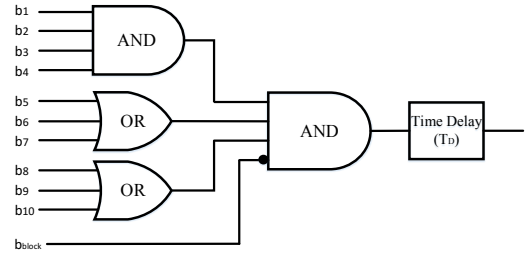

Fig. 7. Decision Logic in the proposed HIF detection logic.

1) DFT-based assertion bits. The four bits go through an AND gate. If any of the four signals are not asserted, the decision logic will not be set high.
2) KF-estimated in-phase components of third harmonic voltage. If none of the three-phase in-phase components of third harmonic estimated from the KF gets asserted, the decision logic will not be set high.
3) KF-estimated in-quadrature components of harmonic voltage. If none of the three-phase in-quadrature components of third harmonic estimated from the KF gets asserted, the decision logic will not be set high.

4) The blocking bit b_{block}. If this bit is 1, the detection logic is blocked and none of HIF events can be detected; if this bit is 0, HIF detection is enabled.

A time delay of T_D is implemented because an appropriate selection of T_D can effectively avoid the false operation resulting from normal switching, which sometimes contributes to third harmonics. The output of the HIF logic is either alarming or tripping signal.

D. Performance Test of the Proposed HIF Detection Logic

1) Testing Environment: The proposed HIF detection logic is tested under 7884 new scenarios: 7776 unbalanced faults and 108 non-faults. The fault locations under testing include faults near B-3, B-11, and B-19. The detailed analysis regarding fault locations can be found in Section V-B3. Similar to the work in [5] and [12], the measurement point is at the substation. Its sampling frequency is 2000 Hz. The time delay in Fig. 7 is set to 100 ms. The average fault detection time is 0.126 sec using OPAL-RT real-time simulator. The signals measured are the three-phase voltage and current. The features used are derived from the measured signals and can be found in the EFS in the unbalanced fault row of Table IV.

2) Testing Criteria: In order to compare the proposed technique with some existing ones in the field, we adopt some of the criteria in [19], [37], including the accuracy (A), dependability (D), security (S), speed (V), objectivity (OBJ), and completeness (COM). The detailed definition of these evaluation criteria is shown in Appendix C. We compare the performance of the proposed method with four representative HIF detection methods in [5], [16], [37], [38], as well as the combined conventional relay elements (including frequency, over/under voltage, over current) in Table VII. The methods in the comparison group cover logic-gate based HIF detector, wavelet domain analysis, time-frequency domain analysis, and pattern recognition techniques.

TABLE VII
HIF DETECTION LOGIC PERFORMANCE COMPARISON.

Solution under test	A (%)	D (%)	S (%)	V	OBJ	COM
The proposed EFS and HIF detection logic	97.0	98.3	95.7	0.13	No	Yes
The work in [5]	N/A	69.0	90.7	N/A	No	Yes
The work in [16]	96	90	100	0.25	No	No
The work in [37]	93.6	100	81.5	1.00	Yes	Yes
The work in [38]	94.9	90.0	90.9	0.11	No	Yes
Combined conventional relay elements	49.1	0.0	98.2	N/A	Yes	Yes

Note: N/A stands for "Not Available" in this table.

3) Performance Comparison: Comparing with the other five methods in Table VII, it is indicated that the proposed method has a superior overall performance in terms of the six evaluation criteria. For example, the detection accuracy of the proposed method is the highest among the solutions under test; its detection speed ($1/60/0.126 = 0.13$, according to Appendix C) is not the fastest but fits well in the HIF detector

requirements on response time [1]. The detection time of less than 1 second, which means the minimum speed of 0.017 in a 60 Hz network is viewed as a conservative setting [12].

4) Security Performance Under Inrush Currents: Inrush currents resulting from transformer energization and motor starting are investigated in this subsection. We have modified the benchmark system in Fig. 4 by integrating a three-phase 500 kVA transformers at L-2, as well as three 500 hp induction motors (the stator windings in delta configuration) at L-3, L-10, L-24. Consequently, aligned with Table IV, the number of transformer energization events is $4 \times 8 \times 3 = 96$ (four inception angles $0°, 45°, 90°, 135°$, eight loading conditions, and three system configurations); the number of motor starting events is $3 \times 8 \times 3 = 72$ (three event locations, eight loading conditions, and three system configurations). Table VIII demonstrates the security index under these two types of events. Based on the results, the proposed technique has very high security performance and therefore can effectively avoid false tripping under inrush currents.

TABLE VIII
SECURITY PERFORMANCE OF THE PROPOSED HIF DETECTION LOGIC UNDER INRUSH CURRENTS.

Non-fault Event Type	Number of Events	S (%)
Transformer energization	96	100
Motor starting	72	100

5) Noise Immunity Capability: Environmental noise can potentially cause false tripping for the HIF detection techniques. The performance of the HIF detection logic under white noise conditions of $5, 10$, and 20 dB is tested. The test is similar to the Out-of-Band test defined in IEEE Standard C37.118.1 for PMUs. The testing scenarios in Section IV-D1 are repeated in MATLAB with the three types of noise conditions added on the measurement.

It is found that the obtained results are closely matching the ones in Table VII. The proposed technique is designed to be immune to noise for the following reasons. Firstly, the signal processing techniques in both DFT and KF blocks in Fig. 5 are equipped with band-pass filters that pass frequencies within a certain range and suppress noise occurring beyond the filters bandwidth. Secondly, as discussed in Section IV-A, the system characteristic averager is implemented with a limiter for each signal channel to avoid signal spikes. The proper selection of the time constant $\bar{T}$ can also help mitigate this issue. Thirdly, both the proposed detection logic and the machine learning model to be tested in the next section are immunized to the noise by itself because they are statistically reliable and the spikes no matter from noise or from derivatives cannot trigger the whole detection logic or the machine learning model. Fourthly, since the high frequency noise is typically very short (few cycles), the time delay that is implemented in the decision

[1] According to [1], to the degree that a utility's service personnel can provide very fast response, there may be less need to de-energize a feeder with a suspected downed conductor. On the other hand, should the decision be made to trip, the fast response by service personnel to isolate the faulted section and restore the remainder of the feeder would minimize the effects of de-energizing.

logic (Fig. 7) can help distinguish high frequency noise from HIFs. In sum, if a certain environmental situation is able to compromise the security, the aforementioned points should be satisfied simultaneously. In sum, if a certain environmental situation is able to compromise the security, the aforementioned points should be satisfied simultaneously.

V. PERFORMANCE ANALYSIS

Performance analysis includes the most commonly occurring single-line-to-ground-fault, the fault scenario analysis, and the testing results.

A. Single-line-to-ground Fault Analysis

Typical waveforms of the proposed EFS upon single-line-to-ground fault are shown in this subsection. A single-line-to-ground HIF is applied in a hybrid distributed generation system (refer to Fig. 4) when $t = 0.3$ second. Fig. 8 shows a representative waveform among EFS.
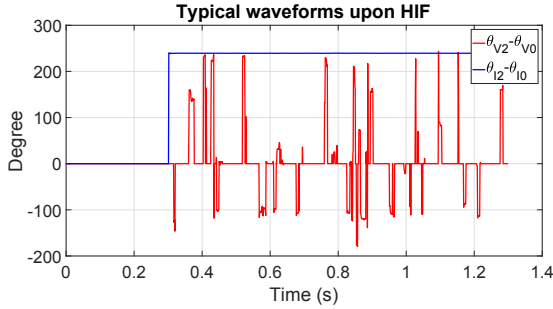

Fig. 8. Typical waveforms angle difference between zero and negative sequence voltage and current under HIF.

B. Fault Scenario Analysis

We evaluate the Effective Feature Set (EFS) in terms of different fault impedances, fault inception angles, and fault locations. The quantifier for evaluation is the variable of importance explained in Section III-A.

1) Fault Impedance: To be practical, this paper investigates the fault impedance up to $500\,\Omega$ to cover typical HIFs whose fault currents are as low as 10 amps. The variable-importance performances of each feature in EFS upon single-line-to-ground (SLG) fault, line-to-line (LL) fault, line-to-line-to-ground (LLG) fault, and three-line-to-ground (LLLG) fault are all depicted. It is concluded that:

- The negative sequence of voltage and current are most reliable features that can keep unaffected during any unbalanced fault upon a varying fault impedance (Fig. 9(a), to be noticed that the dark blue line for V_2 is covered by other lines with the value of 1).
- The feature of the angle difference between negative sequence voltage and zero sequence voltage is reliable under LL faults but vulnerable to high fault impedance under SLG and LLG faults (Fig. 9(a)-(d)).
- The third harmonic components estimated from KF gets deteriorated when the fault impedance increases under SLG and LL faults (Fig. 9(a) and (b)).

- The proposed three-phase HIF detection features are all performing very well except for the fundamental in-quadrature component of current estimated from KF under LLLG faults (Fig. 9(d)).

Furthermore, the proposed algorithm is applicable to unbalanced power systems. Since the employed feature selection method is based on the information gain, what is captured by the information gain is the incremental or variation of the negative sequence signal. Only when the variation pattern of the negative sequence feature contributes to the information gain given the output label belongs to the HIF, does this feature get selected by the proposed algorithm. As a result, the proposed method is applicable to an already unbalanced system.

2) Fault Inception Angle: The effect of fault inception angle is examined as well in this study. The results of unbalanced faults and three phase faults are selectively shown in Fig. 10(a)-(c) respectively. The results in these figures include a varying impedance from 30 Ω to 500 Ω.

The fault inception angle is an insignificant factor that can perturb variable importance. The angles of $30°$ and $60°$ result in a subtle decrease in the variable of importance of the KF estimated third harmonic, but the change is limited. For an LLLG fault, the first order harmonic components of current estimated by KF have a performance drop in non-zero angles.

3) Fault Location: The variable-importance of the features in EFS is presented at three fault locations (bus numbers refer to Fig. 4):

- Location 1: Fault near Bus B-3;
- Location 2: Fault near Bus B-11;
- Location 3: Fault near Bus B-19;

The result is demonstrated in Fig. 10(c), including all fault impedance and all fault inception angles in Table IV. The feature of negative sequence current keeps being unaffected at each location. However, the negative sequence of voltage is so low at location 1 and 2 that the variable of importance becomes almost zero. As the strong voltage source from the substation is ideally balanced, the negative sequence voltage deviation contributed from the HIF is weak. Location 3 is far from the substation, so the negative sequence voltage becomes a good HIF indicator again. To a negligible extent, it is similar for the variable of importance performance of other features: the further the fault is, the less compromised the features are.

C. Testing Results of the Effective Feature Set (EFS)

The proposed EFS is tested under the aforementioned conditions in Table IV, but with dataset on different events. 1944 HIF events and another 1944 non-HIF events (they are unnecessary to be the same number) are simulated for the training of the HIF detector. The types of testing events are similar to those of training events, but at different locations or with different parameter values. There are totally 972 HIF and 972 non-HIF events in the testing. In addition, five classical classifiers (Naive Bayes, Support Vector Machine, k-nearest neighbor, decision tree and random forest) from Weka are compared in order to find the best classifier.

The results with the proposed EFS under different classifiers, shown in Table IX, reveal the effectiveness of the feature
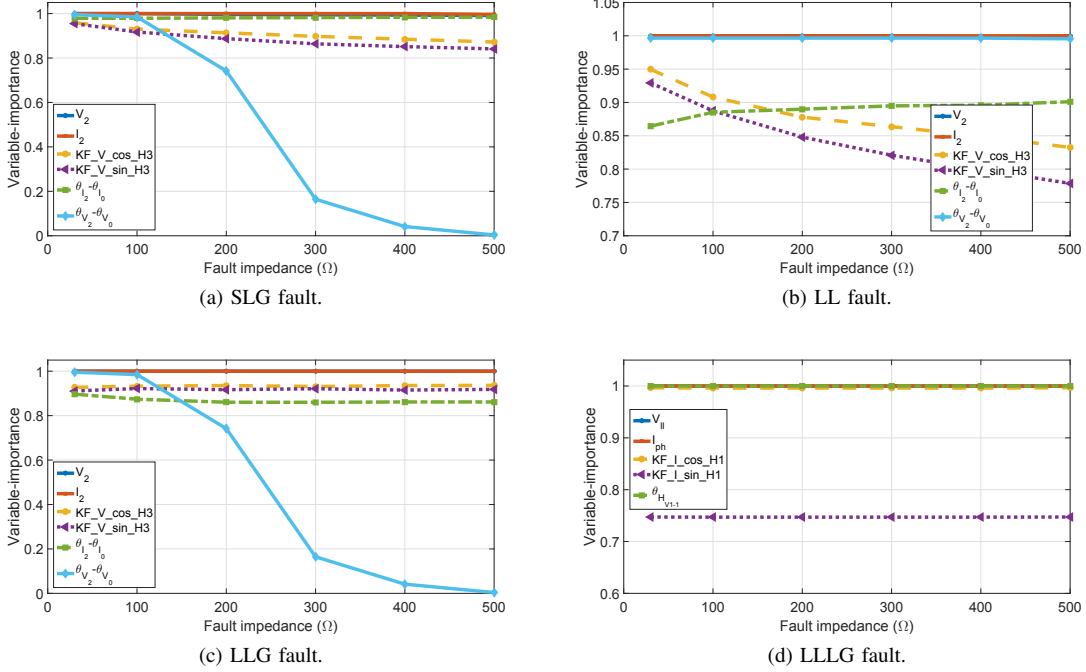
Fig. 9. Variable-importance of all features under faults in a grounded system.

selection. To limit problems such as over-fitting and inaccuracy in prediction, each classifier model is acquired through the 10-folder cross-validation. The performance with Naive Bayes presents the lowest values. The accuracy of the other five classifiers are all above 90%, and remarkably, the performance of the selected artificial neural network (ANN) classifier is exceptionally good. It shows that the proposed EFS works well with most of the non-linear classifiers in HIF detection. However, due to the limited interpretability and debuggability of these classifiers, this paper adopts some linear logic from the tree based classifiers.

TABLE IX
PERFORMANCE OF HIF DETECTION WITH THE EFS WITH DIFFERENT CLASSIFIERS.

Classifier	A (%)	D (%)	S (%)
Naive Bayes	78.0	73.0	82.9
SVM	91.9	89.6	94.1
k-nearest neighbor	98.0	97.7	98.3
Decision Tree	99.4	99.5	99.3
Random Forest	99.7	99.7	99.8
ANN	100.0	100.0	100.0

### D. Discussions on the HIF Detection Logic and Classifiers

Derived from the tree structure of the machine learning classifier model, the proposed HIF detection logic aims to simplify the HIF detection process and be implemented in microprocessor-based relays. The logic complexity of the proposed technique in Fig. 5 is largely reduced. The trade-off here is the HIF detection performance. Fortunately, the discovery of the EFS guarantees a high detection accuracy (97% as shown in Table VII) in the proposed logic. On the other hand, although having excellent HIF detection performance, non-linear classifiers like ANNs is still facing the engineering

challenge to be implemented in the digital relays. The multiple interconnected neurons and layers of ANNs require a higher performance CPU than the one in the digital relays.

The most computationally expensive parts in a machine-learning-based HIF detection algorithm are usually the feature extraction and classifier. In the proposed algorithm, both the features and classifiers are obtained from offline simulation. Therefore, the offline simulation is computationally expensive. An Intel i7 CPU suffices for the majority of HIF detection simulation tasks. If the electric network and operational complexity increase significantly comparing to the system under study, a GPU is required to conduct the offline simulation and obtain the settings. The proposed HIF detection logic, however, does not demand many computational resources and can be integrated into a microprocessor-based relay. Section IV elaborates on the implementation of this logic. If the non-linear classifiers in Table IX are to be implemented in a commercial relay for "real-time" operation, the hardware realization needs to consider a CPU/GPU platform with parallel computation paradigms, a multiply and accumulate operation architecture to deal with the matrix-matrix product of the features and the weights, and a memory hierarchy to store data such as the network weights, etc. [39].

E. Detection Under Low Current Magnitude Levels

The proposed HIF detection technique relies on the time domain features, therefore, its performance can be influenced when the fault current magnitude is low. In the $25\,kV$ benchmark distribution network, the current magnitude in the case study of $500\,\Omega$ fault impedance goes down to $25000/\sqrt{3}/500 = 28.87\,A$. The proposed EFS and HIF detection logic can still maintain a high detection performance (97.0% of accuracy). Further tests indicate that the
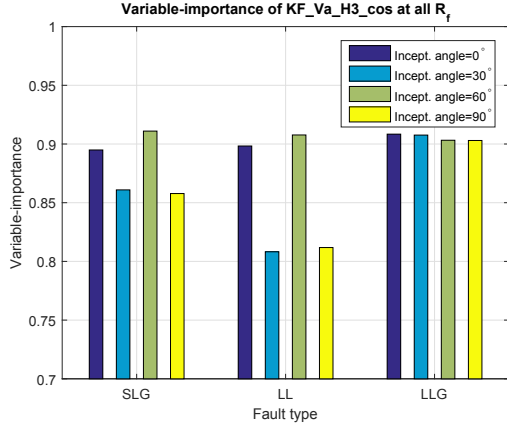
(a) Feature $KF\_V\_cos\_H3$ at different fault inception angles.
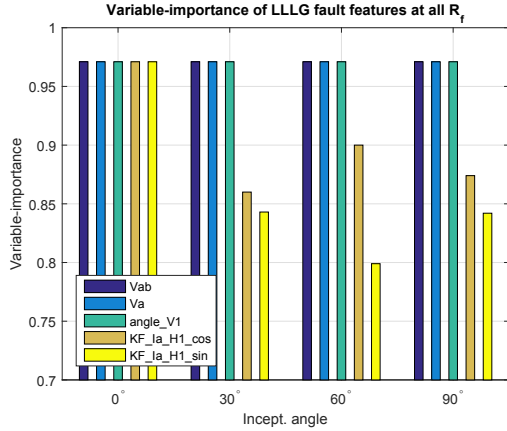
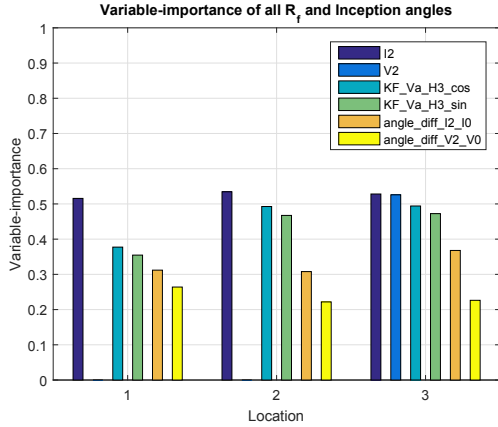(b) LLLG fault features at different fault inception angles.

(c) All R_f at different fault locations.

Fig. 10. Variable-importance at different fault inception angles and locations.

proposed method can detect a fault current down to $14\,\mathrm{A}$ (fault impedance up to $1000\,\Omega$) with the detection accuracy of 87.9%. However, as the fault impedance rises, the variable-importance of some features like $\theta_{V_2} - \theta_{V_0}$ drop significantly (Fig. 9(a)). The precision issue is a problem for many HIF detection techniques. Although the proposed method cannot fully eliminate this problem, two mitigating approaches are recommended: (1) since the proposed technique utilizes the substation as its measurement point, more proposed HIF detectors can be installed along the feeder to receive stronger signals and reduce measurement noise, and (2) measurement devices with higher precision can significantly improve detection performance under lower current magnitude levels.

VI. Conclusions

This paper proposes a new framework for HIF detection and classification. By introducing the MDL-based algorithm to rank a pool of systematically designed features, an effective feature set is generated. The detection capability of such a ranked feature set is evaluated through a comprehensive fault analysis. Furthermore, an applicable logic is recommended based on the extensively used techniques of DFT and KF as well as easily implementable logic gates. It is shown that the proposed method achieves significantly enhanced performance in HIF detection with the effective feature set in different scenarios and that the proposed HIF detection logic exhibits satisfactory dependability, security, and detection time using the real-time simulator.

This paper focuses on 1) proposing an innovative solution to extracting the useful features with advanced machine learning methods, and 2) designing a computational simple HIF detection logic that can be easily translated into relay manufacturing. Admittedly, our lab has not done the physical experiments by far due to the present laboratory condition. In future research, the authors would like to include more physical HIF experiments. The real-world experiment will be helpful to test the proposed method and enhance the practicality.

Appendix A
Derivation of the Minimum Description Length

Assuming that all features are discrete, the objective is to find the best features that maximize the selection measure. Let C, A and V denote the number of classes, the number of features, and the number of values of the given feature. With this notation, we show in the following the entropy of the classes (H_C), the values of the given feature (H_A), the joint events class-feature value (H_{CA}), and the classes given the value of the attribute ($H_{C|A}$).

$$H_C = -\sum_i p_{i.} \log p_{i.}, \qquad H_A = -\sum_j p_{.j} \log p_{.j},$$

$$H_{CA} = -\sum_i \sum_j p_{ij} \log p_{ij}, \qquad H_{C|A} = H_{CA} - H_A,$$

where $p_{ij} = n_{ij}/n_{..}$, $p_{i.} = n_{i.}/n_{..}$, $p_{.j} = n_{.j}/n_{..}$ and $p_{i|j} = n_{ij}/n_{.j}$. "$n_{..}$" denotes the number of training instances and "$n_{i.}$" is the number of training instances from class C_i, $n_{.j}$ is the number of instances with the j-th value of the given attribute, and n_{ij} is the number of instances from class C_i and with the j-th value of the given attribute.

The approximation of the total number of bits that are needed to encode the classes of $n_{..}$ is:

$$\text{Prior MDL}' = n..H_C + \log \binom{n..+C-1}{C-1}, \tag{5}$$

and the approximation of the number of bits to encode the classes of examples in all subsets corresponding to all values of the selected attribute is:

$$\text{Post MDL}' = \sum_j n_{\cdot j} H_{C|j} + \sum_j \log \binom{n_{\cdot j}+C-1}{C-1} + \log A.$$

The last term ($\log A$) is needed to encode the selection of an attribute among A attributes. However, this term is constant for a given selection problem and can be ignored. The first term equals $n_{\cdot\cdot} H_{C|A}$. Therefore, the MDL$'$ measure evaluates the average compression (per instance) of the message by an attribute. The measure is defined by the following difference, Prior MDL$'$ − Post MDL$'$, normalized with $n_{\cdot\cdot}$:

$$\text{MDL}' = \text{Gain} + \frac{1}{n_{\cdot\cdot}} \Big(\log \binom{n_{\cdot\cdot}+C-1}{C-1} \tag{6}$$
$$- \sum_j \log \binom{n_{\cdot j}+C-1}{C-1} \Big). \tag{7}$$

However, entropy H_C can be used to derive MDL$'$ if the messages are of arbitrary length. If the length of the message is known, the more optimal coding uses the logarithm of all possible combinations of class labels for given probability distribution:

$$\text{Prior MDL} = \binom{n_{\cdot\cdot}}{n_{1_\cdot},...,n_{C_\cdot}} + \log \binom{n_{\cdot\cdot}+C-1}{C-1} \tag{8}$$

Similarly, if we use the priori minus the posterior of the MDL, (1) is obtained. The MDL value in (1) is the evaluation index we deployed for the variable-importance approach.

Appendix B
Feeder loading per phase of the system under study

TABLE X
System Configuration under Different DER Technologies.

Phase	Active power (kW)	Reactive power (kVar)
A	3,297	745
B	3,052	671
C	4,425	987
Total	10,774	2,403

Appendix C
Definition to the HIF Detection Evaluation Criteria

We borrow the concepts of true positive (TP), true negative (TN), false positive (FP), and false negative (FN) from statistical classification, and define them and their related evaluation criteria [37] as follows:

- TP: the number of correctly detected fault events.
- TN: the number of correctly detected non-fault events.
- FP: the number of incorrectly detected fault events but they are actually non-fault events.
- FN: the number of incorrectly detected non-fault events but them are actually fault events.
- Accuracy: $A = \frac{TP+TN}{TP+FP+TN+FN}\%$.
- Dependability: $D = \frac{TP}{TP+FN}\%$.

- Security: $S = \frac{TN}{TN+FP}\%$.
- Speed: $V = \frac{T_{one-cycle}}{T_{detection}}\%$, where $T_{one-cycle}$ and $T_{detection}$ are the time duration of one cycle and the detection time respectively.
- Objectivity (OBJ): the objectivity to fault type and network, indicating whether the technique is objective to the type of fault, and the network topology.
- Completeness (COM): the ability to hold important information, indicating the time window of the data that is needed for the method to make the crucial decision for HIF.

References

[1] J. Tengdin and R. Westfall. (1994) High Impedance Fault Detection Technology Report of PSRC Working Group D15. [Online]. Available: http://grouper.ieee.org/groups/td/dist/documents/highz.pdf

[2] J. Carr, "Detection of high impedance faults on multi-grounded primary distribution systems," *Power Apparatus and Systems, IEEE Transactions on*, vol. 100, no. 4, pp. 2008–2016, 1981.

[3] M.-S. Choi, S.-J. Lee, D.-S. Lee, and B.-G. Jin, "A new fault location algorithm using direct circuit analysis for distribution systems," *Power Delivery, IEEE Transactions on*, vol. 19, no. 1, pp. 35–41, 2004.

[4] J. Zhu, D. L. Lubkeman, and A. A. Girgis, "Automated fault location and diagnosis on electric power distribution feeders," *Power Delivery, IEEE Transactions on*, vol. 12, no. 2, pp. 801–809, 1997.

[5] D. C. Yu and S. H. Khan, "An adaptive high and low impedance fault detection method," *Power Delivery, IEEE Transactions on*, vol. 9, no. 4, pp. 1812–1821, 1994.

[6] W. H. Kwon, G. W. Lee, Y. M. Park, M. C. Yoon, and M. H. Yoo, "High impedance fault detection utilizing incremental variance of normalized even order harmonic power," *Power Delivery, IEEE Transactions on*, vol. 6, no. 2, pp. 557–564, 1991.

[7] J. R. Macedo, J. W. Resende, C. A. Bissochi, D. Carvalho, and F. C. Castro, "Proposition of an interharmonic-based methodology for high-impedance fault detection in distribution systems," *Generation, Transmission & Distribution, IET*, vol. 9, no. 16, pp. 2593–2601, 2015.

[8] A. A. Girgis, W. Chang, and E. B. Makram, "Analysis of high-impedance fault generated signals using a kalman filtering approach," *Power Delivery, IEEE Transactions on*, vol. 5, no. 4, pp. 1714–1724, 1990.

[9] K. Sagastabeitia, I. Zamora, A. Mazón, Z. Aginako, and G. Buigues, "Low-current fault detection in high impedance grounded distribution networks, using residual variations of asymmetries," *Generation, Transmission & Distribution, IET*, vol. 6, no. 12, pp. 1252–1261, 2012.

[10] N. I. Elkalashy, M. Lehtonen, H. A. Darwish, A.-M. I. Taalab, and M. A. Izzularab, "Dwt-based detection and transient power direction-based location of high-impedance faults due to leaning trees in unearthed mv networks," *Power Delivery, IEEE Transactions on*, vol. 23, no. 1, pp. 94–101, 2008.

[11] M. Haghifam, A. Sedighi, and O. Malik, "Development of a fuzzy inference system based on genetic algorithm for high-impedance fault detection," *IEE Proceedings Generation Transmission and Distribution*, vol. 153, no. 3, pp. 359 – 367, 2006.

[12] S. Gautam and S. M. Brahma, "Detection of high impedance fault in power distribution systems using mathematical morphology," *Power Systems, IEEE Transactions on*, vol. 28, no. 2, pp. 1226–1234, 2013.

[13] C. Kim, B. D. Russell, and K. Watson, "A parameter-based process for selecting high impedance fault detection techniques using decision making under incomplete knowledge," *Power Delivery, IEEE Transactions on*, vol. 5, no. 3, pp. 1314–1320, 1990.

[14] C. Kim and B. D. Russell, "A learning method for use in intelligent computer relays for high impedance faults," *Power Delivery, IEEE Transactions on*, vol. 6, no. 1, pp. 109–115, 1991.

[15] Y. Sheng and S. M. Rovnyak, "Decision tree-based methodology for high impedance fault detection," *Power Delivery, IEEE Transactions on*, vol. 19, no. 2, pp. 533–536, 2004.

[16] A.-R. Sedighi, M.-R. Haghifam, O. Malik, and M.-H. Ghassemian, "High impedance fault detection based on wavelet transform and statistical pattern recognition," *Power Delivery, IEEE Transactions on*, vol. 20, no. 4, pp. 2414–2421, 2005.

[17] T. Lai, L. Snider, E. Lo, and D. Sutanto, "High-impedance fault detection using discrete wavelet transform and frequency range and rms conversion," *Power Delivery, IEEE Transactions on*, vol. 20, no. 1, pp. 397–407, 2005.

[18] M. Sarlak and S. M. Shahrtash, "High-impedance faulted branch identification using magnetic-field signature analysis," *Power Delivery, IEEE Transactions on*, vol. 28, no. 1, pp. 67–74, 2013.

[19] A. Ghaderi, H. L. Ginn III, and H. A. Mohammadpour, "High impedance fault detection: a review," *Electric Power Systems Research*, vol. 143, pp. 376–388, 2017.

[20] Schweitzer Engineering Laboratories. (2013) SEL-421 Relay Protection and Automation System Instruction Manual. [Online]. Available: https://www.eiseverywhere.com/file_uploads/a3f24f026f353ca67887b5c2df49bc7e_SEL421IM.pdf

[21] Visimax Technologies Inc. (2015) Phasor Measurement Unit (PMU) Datasheet. [Online]. Available: https://rmspl.com.au/wordpress/wp-content/uploads/2015/04/VIZIMAX-PMU010000-SP-en-20151007-PMU-datasheet.pdf

[22] D. C. T. Wai and X. Yibin, "A novel technique for high impedance fault identification," *Power Delivery, IEEE Transactions on*, vol. 13, no. 3, pp. 738–744, 1998.

[23] M. Kizilcay and T. Pniok, "Digital simulation of fault arcs in power systems," *Electrical Power, European Transactions on*, vol. 1, no. 1, pp. 55–60, 1991.

[24] W. Zhang, Y. Jing, and X. Xiao, "Model-based general arcing fault detection in medium-voltage distribution lines," *Power Delivery, IEEE Transactions on*, vol. 31, no. 5, pp. 2231–2241, 2016.

[25] A. Emanuel, D. Cyganski, J. Orr, S. Shiller, and E. Gulachenski, "High impedance fault arcing on sandy soil in 15 kv distribution feeders: contributions to the evaluation of the low frequency spectrum," *Power Delivery, IEEE Transactions on*, vol. 5, no. 2, pp. 676–686, 1990.

[26] N. I. Elkalashy, M. Lehtonen, H. A. Darwish, M. A. Izzularab, and I. T. Abdel-maksoud, "Modeling and experimental verification of high impedance arcing fault in medium voltage networks," *Dielectrics and Electrical Insulation, IEEE Transactions on*, vol. 14, no. 2, pp. 375–383, 2007.

[27] Q. Cui, K. El-Arroudi, and G. Joós, "Islanding detection of hybrid distributed generation under reduced non-detection zone," *IEEE Transactions on Smart Grid*, vol. 9, no. 5, pp. 5027–5037, 2018.

[28] L. Ming and P. Vitányi, *An introduction to Kolmogorov complexity and its applications*. Springer Heidelberg, 1997.

[29] N. V. Chawla, K. W. Bowyer, L. O. Hall, and W. P. Kegelmeyer, "Smote: synthetic minority over-sampling technique," *Journal of artificial intelligence research*, vol. 16, pp. 321–357, 2002.

[30] S. Huang, L. Luo, and K. Cao, "A novel method of ground fault phase selection in weak-infeed side," *IEEE Transactions on Power Delivery*, vol. 29, no. 5, pp. 2215–2222, Oct 2014.

[31] H. Laaksonen and P. Hovila, "Method for high-impedance fault detection," *CIRED - Open Access Proceedings Journal*, vol. 2017, no. 1, pp. 1295–1299, 2017.

[32] I. Kamwa, S. R. Samantaray, and G. Joos, "Compliance analysis of pmu algorithms and devices for wide-area stabilizing control of large power systems," *IEEE Transactions on Power Systems*, vol. 28, no. 2, pp. 1766–1778, May 2013.

[33] Schweitzer Engineering Laboratories. (2016) Arc Sense Technology (AST) High-Impedance Fault Detection. [Online]. Available: https://cdn.selinc.com/assets/Literature/Product%20Literature/Flyers/Arc-Sense_PF00160.pdf?v=20161031-073656

[34] B. D. Russell Jr, "High impedance fault detection apparatus and method," Aug. 14 1984, US Patent 4,466,071.

[35] J. L. Blackburn and T. J. Domin, *Protective relaying: principles and applications*. CRC press, 2006.

[36] D. Hou, "Detection of high-impedance faults in power distribution systems," in *Power Systems Conference: Advanced Metering, Protection, Control, Communication, and Distributed Resources*. IEEE, 2007, pp. 85–95.

[37] A. Ghaderi, H. A. Mohammadpour, H. L. Ginn, and Y.-J. Shin, "High-impedance fault detection in the distribution network using the time-frequency-based algorithm," *Power Delivery, IEEE Transactions on*, vol. 30, no. 3, pp. 1260–1268, 2015.

[38] S. Sahoo and M. E. Baran, "A method to detect high impedance faults in distribution feeders," in *T&D Conference and Exposition, 2014 IEEE PES*. IEEE, 2014, pp. 1–6.

[39] V. Sze, Y.-H. Chen, J. Emer, A. Suleiman, and Z. Zhang, "Hardware for machine learning: Challenges and opportunities," in *2017 IEEE Custom Integrated Circuits Conference (CICC)*. IEEE, 2017, pp. 1–8.
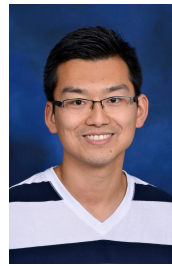
Qiushi Cui (S'10-M'18) received the M.Sc. degree from Illinois Institute of Technology, and the Ph.D. degree from McGill University, both in Electric Engineering. Currently, he is a postdoctoral scholar of electrical engineering in the Ira A. Fulton Schools of Engineering of Arizona State University (ASU). Prior to joining ASU, he was a research engineer and held a Canada MITACS Accelerate Research Program Fellowship at OPAL-RT Technologies Inc. from 2015 to 2017.

His research interests are in the areas of machine learning and big data applications in power systems, power system protection, smart cities, microgrid, EV integration, renewable energies, and real-time simulation in power engineering. Dr. Cui won the Best Paper Award at the 13th IET International Conference in Developments in Power System Protection in Edinburgh, UK, in 2016. He was the winner of the Chunhui Cup Innovation and Entrepreneurship Competition for Overseas Chinese Scholars in Energy Sector in 2018.

Khalil El-Arroudi (S'99-M'06) received the B.Sc and M.Sc. degrees from Garyounis University, Libya, and the Ph.D. degree from McGill University, Canada, in 1986, 1994, and 2004 respectively. He has twenty-three years of experience in power system protection, and system operation. At the General Electricity Company of Libya (GECOL), he has occupied different managerial positions including the General Manager of System Operation, and the Chairman and Managing Director.

He has been a member and chair in different international Mediterranean interconnection committees including the LTAM-ENTSOE interconnection (Maghrebian-European projects), the Arab Union of Electricity, the Mediterranean Electricity Network (MEDELEC), and the OME (Observatoire Méditerranéen de lÉnergie). He holds two USA Patents US8200372B2 related to transmission systems and distributed generations. His research interests include power system protection, distributed generation applications, microgrids, smart grids, and applications of intelligent applications in power systems.

Yang Weng (M'14) received the B.E. degree in electrical engineering from Huazhong University of Science and Technology, Wuhan, China; the M.Sc. degree in statistics from the University of Illinois at Chicago, Chicago, IL, USA; and the M.Sc. degree in machine learning of computer science and M.E. and Ph.D. degrees in electrical and computer engineering from Carnegie Mellon University (CMU), Pittsburgh, PA, USA.

After finishing his Ph.D., he joined Stanford University, Stanford, CA, USA, as the TomKat Fellow for Sustainable Energy. He is currently an Assistant Professor of electrical, computer and energy engineering at Arizona State University (ASU), Tempe, AZ, USA. His research interest is in the interdisciplinary area of power systems, machine learning, and renewable integration.

Dr. Weng received the CMU Deans Graduate Fellowship in 2010, the Best Paper Award at the International Conference on Smart Grid Communication (SGC) in 2012, the first ranking paper of SGC in 2013, Best Papers at the Power and Energy Society General Meeting in 2014, ABB fellowship in 2014, and Golden Best Paper Award at the International Conference on Probabilistic Methods Applied to Power Systems in 2016.